PROCEEDINGS, 48th Workshop on Geothermal Reservoir Engineering
Stanford University, Stanford, California, February 6-8, 2023
SGP-TR-224

Permeability-Related Spatial Correlation Systematics for FORGE EGS Stimulation MEQs

Peter Leary and Peter Malin

Advanced Seismic Instrumentation and Research

pcl@asirseismic.com pem@asirseismic.com

Keywords: Meqs, EGS, stimulation, ambient crust, lognormality, spatial correlation, two-point correlation

ABSTRACT

UtahForge Well 16A(78)-32 stimulation Meq XYZM (location/magnitude) data are processed to show two spatial correlation features observed in ambient crust Meqs: lognormal moment distributions and event-pair spatial correlation scaling with inter-event offset r, $G(r) \sim 1/r^p$, $p \sim 1$. Neither spatial correlation feature is compatible with uncorrelated randomness typically assumed for spatially averaged crustal heterogeneity and/or DFN distributions. Both UtahForge Meq spatial correlation features are, however, congruent with rock-fluid interaction spatial-correlation empirics attested by ambient crust well-log, well-core, and well-flow data worldwide. UtahForge Meq spatial correlation features are seen to apply equally to ambient crustal Meqs recorded at tectonic, convective geothermal, and crystalline basement EGS stimulation sites. More specifically, the UtahForge Meq spatial correlations are latent in the ambient crust poro-permeability relation $\kappa(x,y,z) \sim \exp(\alpha\varphi(x,y,z))$, where porosity $0 < \varphi(x,y,z) < 1$ is a pink-noise random power-law scaling volumetric distribution and α a poro-connectivity parameter with empirical value range $2\text{-}3 < \alpha\underline{\varphi} < 5\text{-}6$ for crustal formations with mean porosities $0.003 < \underline{\varphi} < 0.3$. The poro-permeability relation $\kappa(x,y,z) \sim \exp(\alpha\varphi(x,y,z))$ is inherently lognormal for the empirical $\alpha\underline{\varphi}$ condition, with high-end permeability sites spatially correlated as $G(r) \sim 1/r^p$, $p \sim 1$. It follows that many if not most UtahForge stimulation Meqs, in line with ambient crust Meqs elsewhere, arise from low-velocity seismic slip within high permeability poro-connectivity structures rather than as high velocity slip on planar fault surfaces. Meq moment distributions thus reflect ambient crust permeability structures, while hectohertz seismic emission waveform spectra and coda scattering of crustal basement stimulation Meqs provide support evidence for seismic slip on poro-permeability structures given by the $\kappa(x,y,z) \sim \exp(\alpha\varphi(x,y,z))$ ambient crust rock-fluid interaction empiric.

1. INTRODUCTION

The three UtahForge stimulation stages of Meq XYZM data processed here are available as xlsx spreadsheets at Seismic Data from the Well 16A(78)-32 Stimulation April, 2022 DOI 10.15121/1879450. Data processing applied to the appended Stage 1 XYZM1 text file illustrates the details of poro-permeability spatial correlation phenomenology latent in ambient crust Meq XYZM distributions. Accompanying the Meq data processing are model spatial correlation distributions for spatially uncorrelated (white noise) and spatially correlated (pink noise) numerical realisations of the ambient crust poroperm empiric $\kappa(x,y,z) \sim \exp(\alpha\varphi(x,y,z))$.

Similarly processed Meq XYZM data from diverse locations support the lognormal moment distributions and two-point event-pair spatial correlations $G(r) \sim 1/r^p$, $p \sim 1$. Readily available examples are from EGS stimulation Meqs at 6km depth in Finnish basement, background seismicity from the southern California seismic network, and Indonesia convective geothermal Meq activity. Lognormal Meq moment distributions are evident in 1960s USGS oil field monitoring Meq data from Rangely CO and for Parkfield Meqs on the San Andreas fault. Finnish basement EGS stimulation Meq waveforms recorded at 2.5km depth show both spectral distributions and coda wave scattering systematic directly attributable to ambient crustal poro-permeability structures $\kappa(x,y,z) \sim \exp(\alpha\varphi(x,y,z))$.

Logical inferences drawn from available Meq XYZM data are:

- The UtahForge Stage 1-3 data acquisition and processing accurately reflect ambient crust physical reality latent in abundant well-log, well-core, and well-flow data worldwide.
- Meq XYZM spatial correlation systematics refute modeling assumptions that ambient crustal flow and Meq slip processes arise from media in which spatial variations are uncorrelated and can consequently be approximated as poro-elastic continua with properties given by spatially averaged small-scale/sparse sampling.
- Present UtahForge Stage 1-3 data acquisition and processing facilities are a blue-print for developing more intensive seismic monitoring facilities built and operated on the guide-line that ambient crust heterogeneity attested by well-log, well-core and well-flow empirics is reflected by the Meq ~ Permeability statistical congruence, whence well-located Meqs offer by far the best chance to understand, develop, and achieve EGS permeability stimulation goals.

2. UTAH FORGE STAGE 1 MEQ SPATIAL CORRELATION PROCESSING IN MATLAB

The following sequence of Matlab commands uses the appended short UtahForge Stage 1 Meq XYZM data to illustrate the spatial correlations latent in ambient crust Meq distributions. Processing the longer UtahForge Stage 2-3 Meq data, along with Meq XYZM data from elsewhere in the ambient crust, follows the same Matlab command sequence.

```
x=XYZM1(:,1); y=XYZM1(:,2);z=XYZM1(:,3);m=XYZM1(:,4);  % appended XYZM text file
figure(1);clf
plot3(x-mean(x),y-mean(y),z-mean(z),'*');grid;axis  equal;view(3)
```

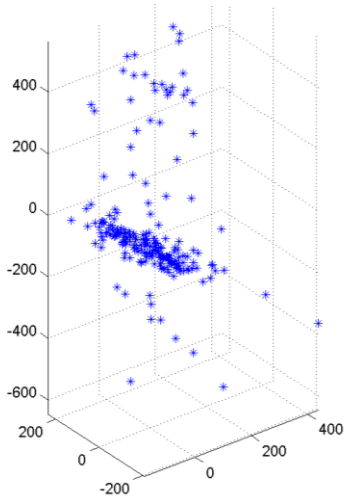

Figure 1: UtahForge Stage 1 XYZM data Meq locations

```
figure(2);clf;hold  on
M=exp(m);[hn,hx]=hist(M,20); % distribution of Meq moments M = exp(m)
bar(hx-min(hx),hn/max(hn))  % plot normalised moment distribution
n=randn(1e6,1);n=.1+.2*(n-min(n))/(max(n)-min(n));  % numerical porosities 0. 1 < n < 0.3
a=17;k=exp(a*n); % associated empirical permeabilities k for a = 17; a*mean(n) ~ 3
[hnk,hxk]=hist(k,20); hxk=hxk-min(hxk);  % normalised permeability distribution
plot(hxk/max(hxk),hnk/max(hnk),'r','LineWidth',3);  % overlay permeability/moment distributions
axis([0 1 0 1]);title(['LOGNORMAL EXP(\alpha\phi)    \alpha = ',int2str(a)]);grid
```

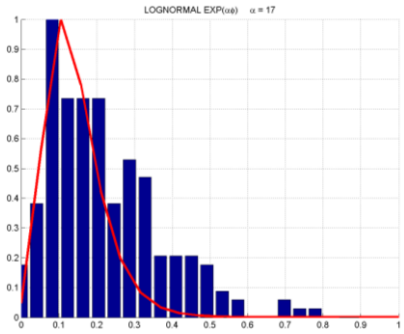

Figure 2: UtahForge Stage 1 XYZM data Meq moment lognormal distribution (blue) with numerical lognormal distribution (red) given by $\kappa(x,y,z) \sim \exp(\alpha\varphi(x,y,z))$ realised by spatially correlated porosity normal distribution $0 < \varphi(x,y,z) < 0.3$ with mean value $\underline{\varphi} \sim 0.2$ and poro-connectivity parameter $\alpha \sim 17$, meeting the empirical condition $2\text{-}3 < \alpha\underline{\varphi} < 5\text{-}6$.

```
nx=length(x);
for i=1:nx for j=1:nx rsq(i,j)=(x(i)-x(j)).^2+(y(i)-y(j))^2+(z(i)-z(j))^2; end;end;r=sqrt(rsq);
figure(3);hist(r(:),100)
```

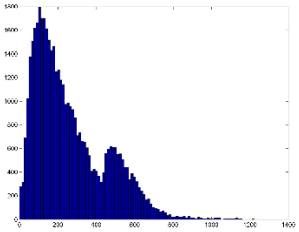

Figure 3: Distribution of Meq XYZM event-pair offsets 0 < r < 1000. Secondary bump reflects existence of event subcluster; subsequent processing is restricted to event-pair offsets r < 400.

```
Inz=find(r>0 & r<400);[hn,hx]=hist(r(Inz),100);hn=hn+1;

q=1:25;c=polyfit(log(hx(q)),log(hn(q)./hx(q).^2),1);s=polyval(c,log(hx(q)));

figure(4);clf;subplot(211);loglog(hx,hn./hx.^2,'.',hx(q),exp(s),'r','LineWidth',3);grid;

xlabel('PAIR-OFFSET (5M-400M)');ylabel('PAIR-COUNT');title(['G(R) ~ 1/R^P P = ',num2str(-c(1),3)])

Inz=find(r>0 & r<100); [hn,hx]=hist(r(Inz),100);hn=hn+1;

q=1:100;c=polyfit(log(hx(q)),log(hn(q)./hx(q).^2),1);s=polyval(c,log(hx(q)));

subplot(212);loglog(hx,hn./hx.^2,'.',hx(q),exp(s),'r','LineWidth',3);grid;

xlabel('PAIR-OFFSET (5M-100M)');ylabel('PAIR-COUNT');title(['G(R) ~ 1/R^P P = ',num2str(-c(1),3)])
```

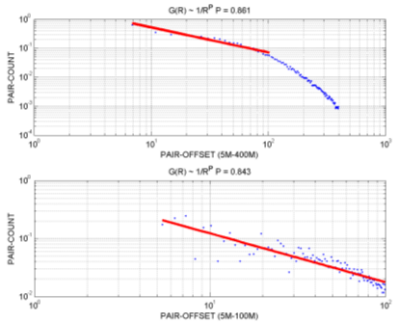

Figure 4: Power-law scaling Stage 1 Meq XYZM event-pair spatial correlation frequency distribution $G(r) \sim 1/r^p$, $p \sim 0.85$, for 5m-400m offset range (above) and 5m-100m offset range (below). Both scaling exponents approximate the expected value $p \sim 1$; the smaller value is due to statistical event location error. The standard Meq assumption of uncorrelated event randomness requires a null correlation exponent $p \sim 0$.

3. NUMERICALLY REALISED PAIR-WISE SPATIAL CORRELATION DISTRIBUTIONS FOR WHITE AND PINK NOISE

```
%load save_v_150x150x150.mat          % 3D array of pink noise spatially correlated fluctuations

figure(5);imagesc(v(:,:,50));axis equal

v=.1+.2*(v-min(v(:)))/(max(v(:))-min(v(:)));K=exp(20*v);K=K/max(K(:));

figure(6);clf;subplot(211);hist(K(:),1000);grid

Kcut=.45;IK=find(K>Kcut);whos IK

n=0;X=0;Y=0;Z=0;for k=1:150 for j=1:150 for i=1:150 if K(i,j,k)>Kcut n=n+1;X(n)=i;Y(n)=j;Z(n)=k;end;end;end;end

figure(7);plot3(X,Y,Z,'.');grid;axis equal;view(3)

R2=zeros(n);for i=1:n for j=1:n R2(i,j)=(X(i)-X(j)).^2+(Y(i)-Y(j))^2+(Z(i)-Z(j))^2;end;end;R=sqrt(R2);

InzR=find(R>1 & R<225);whos InzR

[hnR,hxR]=hist(R(InzR),100);hnR=hnR+1;
```

```
q=1:25;cR=polyfit(log(hxR(q)),log(hnR(q)./hxR(q).^2),1);sR=polyval(cR,log(hxR(q)));
figure(8);clf;subplot(211);loglog(hxR(q),hnR(q)./hxR(q).^2,'s',hxR(q),exp(sR),'r','LineWidth',3);grid
axis([1e0 1e2 1e0 3e3]);ylabel('PAIR-COUNT');title(['G(R)~ 1/R^P  P = ',num2str(-cR(1),3)])
v=randn(150,150,150);   % 3D array of white noise spatially uncorrelated fluctuations
figure(5);imagesc(v(:,:,50));axis  equal
v=.1+.2*(v-min(v(:)))/(max(v(:))-min(v(:)));K=exp(3*v);K=K/max(K(:));
figure(6);subplot(212);hist(K(:),1000);grid
Kcut=.9;IK=find(K>Kcut);whos IK
n=0;X=0;Y=0;Z=0;for k=1:150 for j=1:150  for i=1:150 if K(i,j,k)>Kcut n=n+1;X(n)=i;Y(n)=j;Z(n)=k;end;end;end;end
figure(7);plot3(X,Y,Z,'.');grid;axis  equal;view(3)
R2=zeros(n);for i=1:n  for j=1:n R2(i,j)=(X(i)-X(j)).^2+(Y(i)-Y(j))^2+(Z(i)-Z(j))^2;end;end;R=sqrt(R2);
InzR=0;InzR=find(R>1 & R<225);whos InzR
hnR=0;hxR=0;[hnR,hxR]=hist(R(InzR),100);hnR=hnR+1;
q=1:15;cR=polyfit(log(hxR(q)),log(hnR(q)./hxR(q).^2),1);sR=polyval(cR,log(hxR(q)));
figure(8);subplot(212);loglog(hxR(q),hnR(q)./hxR(q).^2,'o',hxR(q),exp(sR),'m','LineWidth',3);grid
axis([1e0 1e2 1e0 3e3]);ylabel('PAIR-COUNT');title(['G(R)~ 1/R^P  P = ',num2str(-cR(1),3)])
```

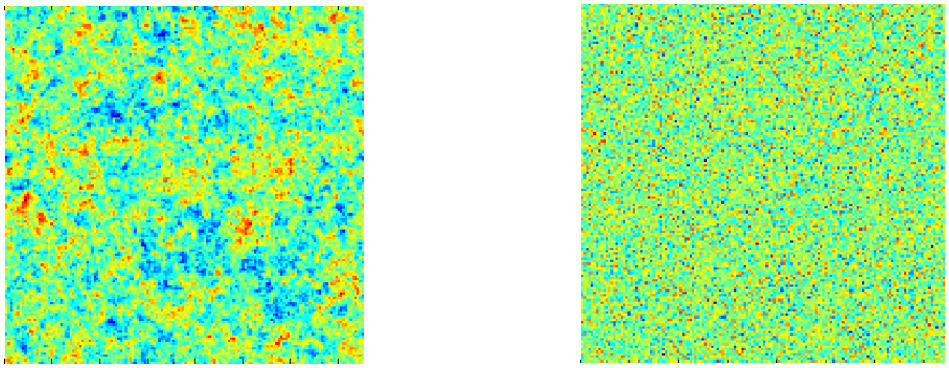

Figure 5: (Left/Right) Pink/white noise section: S(k)~1/k, S(k)~const

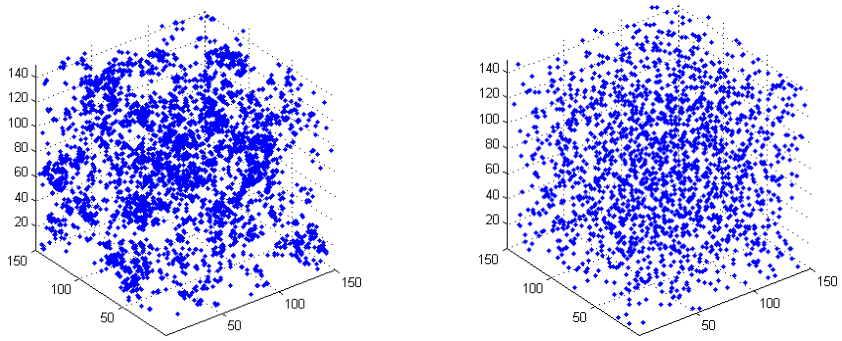

Figure 6; (Left/Right) Pink/white noise event spatial correlation/non-correlation.

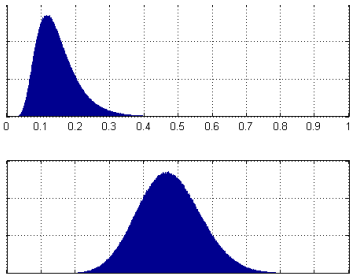

Fig 7 – (Above/Below) Pink/white noise distributions: lognormal;/normal.

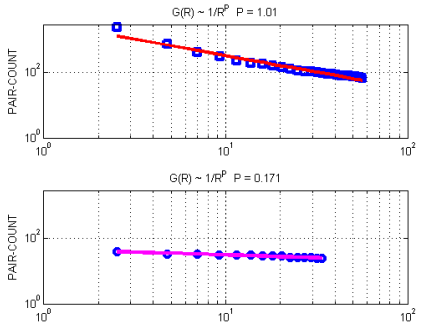

Figure 8: (Above/Below) Pink/white two-point pair-wise spatial correlation functions for pair-offset R, G(R) ~ $1/R^P$, P ~ 1/0.

4. UTAH FORGE STAGE 1-3 MEQ LOGNORMAL-MOMENT/TWO-POINT-SPATIAL CORRELATION DISTRIBUTIONS

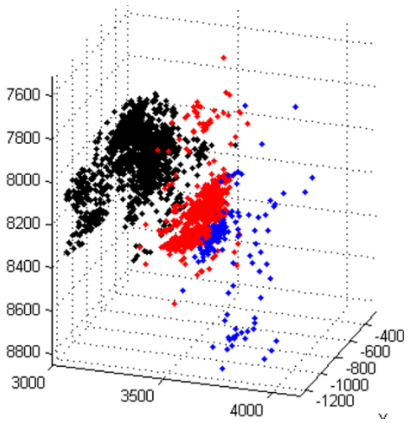

Figure 9: UtahForge Stage 1-3 stimulation Meq event spatial distributions; Stage 1 = blue; Stage 2 = red; Stage 3 = black.

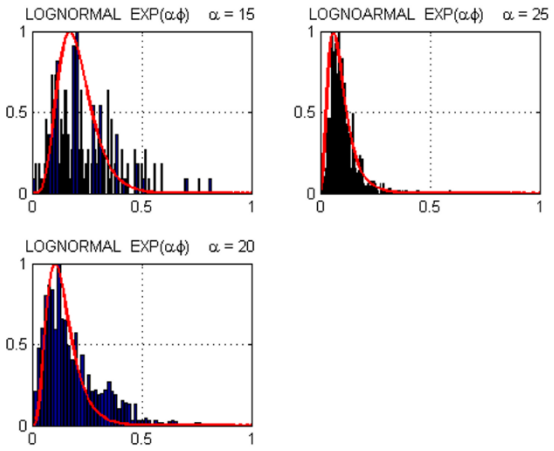

Figure 10: UtahForge Stage 1-3 lognormal Meq moment distributions $\kappa \sim \exp(\alpha\varphi)$ for three values of poro-connectivity parameter $\alpha \sim 15, 25, 20$ realised for pink noise numerical porosity normal distribution $0.1 < \varphi < 0.3$ with mean porosity $\underline{\varphi} \sim 0.2$. The empirical value range for poro-connectivity parameter, $2\text{-}3 < \alpha\underline{\varphi} < 5\text{-}6$, is observed for above values $\alpha \sim 15, 25, 20$.

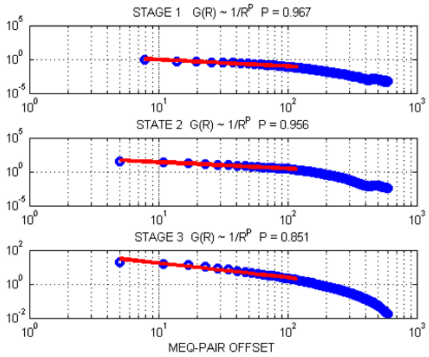

Figure 11: UtahForge Stage 1-3 Meq two-point spatial correlation distributions $G(R) \sim 1/R^P$ for Meq-pair offset R. Observed Meq spatial correlation exponent values near unity, $P \sim 1$, is predicted for Meqs occurring on localised spatial correlation structures with high values of ambient crust poro-permeability.

SCIENCE PERSPECTIVE ON MEQ XYZM SPATIAL CORRELATION SYSTEMATICS

Science advances through making and testing predictions that logically follow from a set of clearly stated assumptions. From this perspective, the decades-long assumption that spatial variations in crustal rock-fluid interactions are spatially uncorrelated must now be abandoned as failing to properly predict crustal flow structure data.

The spatial non-correlation nature of crustal rock-fluid interactions began with the 1850s publication of Darcy/Dupuis groundwater observations calibrated against fluid flow in the unconsolidated sands of municipal water filtration works [1]. The resultant Darcy's Law provided a superior understanding of how aquifer-borne groundwater flow related to gravitational pressure heads than did existing concepts of pipe-flow in the chalk formations of the Paris Basin.

At the centenary of Darcy's Law, Hubbert [2] tried to formalise the Darcy/Dupuis unconsolidated sands picture of fluid flow in rock. Hubbert simply asserted that at length scales above suitably small values (greater than, say, hand-samples) and below suitably large values (less than, say, whole formations), it was statistically proper to spatially average over crustal rock-fluid interaction properties. Within a crustal formation, say, fluid effectively flowed as if there were no small or intermediate scale spatial fluctuations that were not balanced by equally sized but oppositely signed spatial fluctuations. Thus, to first order, and by statistically knowable amounts, crustal fluid flow uncertainty could be managed for groundwater aquifer and hydrocarbon reservoir operation.

Such was the appeal of the Hubbert taming of reservoir flow uncertainty, particularly as it impacted the rapidly advancing promise of computer flow modelling, that Warren [3] introduced his dual-porosity sugar cube reduction of crustal flow heterogeneity, and Bear [4] formulated/popularised the notion of REVs (representative elementary volumes) in computerised flow simulation.

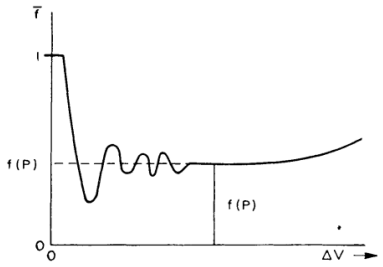

FIG. 5 — Method of defining point values of macroscopic quantities illustrated with the porosity *f*.

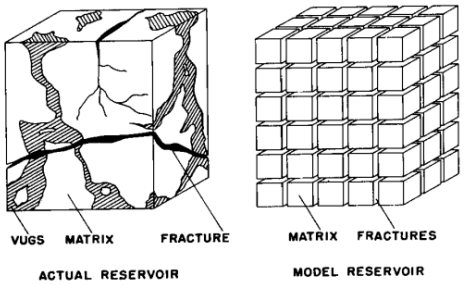

FIG. 1 — IDEALIZATION OF THE HETEROGENEOUS POROUS MEDIUM.

Figure 12: (Left) Sketch of Hubbert [2] assertion for crustal porosity and related flow property spatial fluctuations as function of volumetric scale ΔV: (i) at small scales (e.g., hand samples) can be large in amplitude but can be averaged out; (ii) at intermediate scales are moderate in amplitude but can be averaged out; (iii) at large scales (e.g., formations) to be identified with geological structures and given spatially averaged "effective medium" constant porosity and related flow values. (Right) Sketch of Warren [3] "dual porosity" approximation to geological medium flow spatial complexity in which "sugar cube" permeability and intervening fracture permeability can both differ and vary locally but do not systematically create large scale erratic flow structures that transgress geological boundaries; the sugar cube model persists in TOUGH2 crustal flow code.

With the 1980s advent of digitised well-logs, outright and systematic evidence of the failure of the Hubbert/Warren/Bear statistical hypothesis was at hand. It became clear that well-log fluctuation power-spectra S(k) were not flat/constant for spatial wave-number k as required by the Hubbert/Warren/Bear hypothesis, but instead the power-spectra systematically scaled inversely with spatial wave-number, S(k) ~ 1/k across five to six decades of scale range, 1/km < k < 1/cm, as seen worldwide for porosity, sonic velocity, galvanic properties, and radionuclide-bearing solute mineral distributions [5].

The contradictory spectral scaling S(k) ~ 1/k property attested by well-log data worldwide did not, however, cause hydrocarbon reservoir flow modelers to modify their statistical assumption about spatial fluctuations. As no one found a way to locate hydrocarbon production wells within the newly evident statistically erratic flow structure framework, onshore oil/gas field drilling on a grid remained in practice while offshore oil/gas field drilling laterally followed producer formations. In both cases oil/gas reservoir flow modeling followed suit by ignoring the invalidation of how computer models were populated with crustal flow properties. TOUGH2, by far the most widely used flow modeling code [6], still features the Warren sugar cube figure, and has no provision for encompassing the high degrees of long-range crustal flow property spatial heterogeneities attested by well-log, well-log, and well-flow data for crustal fluid systems observed worldwide.

Neither of the onshore/offshore hydrocarbon drilling options apply to geothermal reservoir development. Essentially blind vertical drilling of convective geothermal flow systems does not have the high-flow hit rate needed to cover drilling costs. Horizontal drilling is too expensive for pay from geothermal waters that have approximately 1% of hydrocarbon pay per unit volume.

The reality of geothermal energy production – need for well flow rates that exceed oil/gas flow rates by two orders of magnitude – demands clear scientific understanding of crustal fluid flow processes [7]. This understanding must recognise that crustal flow is spatially correlated at all scale lengths as mandated by well-log power-spectral scaling S(k) ~ 1/k, 1/km < k < 1/cm. To date, however, UtahForge flow modeling procedures are bound by assuming crustal flow properties are uncorrelated, S(k) ~ const, and can thus be effectively eliminated from either/both conceptual and computational reality as per the Hubbert assertion [2].

An extreme example of the limited nature of this assumption is the following formal modeling computational assessment based on the existence of 1m-wide uniform vertical conductive flow structure sandwiched between two crustal thermal store layers 4km on a side as pictured below [8]:

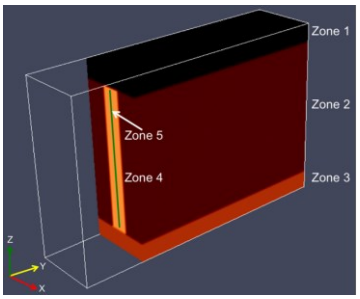

Figure 13: Spatial configuration of a 35MW crustal EGS facility based on a 1m thick high porosity flow section 4km on a side (DOI 10.1186/s40517-015-0033-5). The configuration appears in the following context: "[T]he land surface available for emplacing EGS would support a maximum of 13,450 EGS plants each comprising 18 wells and delivering an average electric power of 35.3 MWe….. [T]hese systems collectively may supply 4155 TWh of electric energy in 1 year…roughly seven times the electric energy produced in Germany in the year 2011."

The Fig 13 flow configurations is conceivable only in a world of engineering manufacturing materials described by spatial fluctuation spectral distributions S(k) ~ const. The fact of ambient crustal rock having flow-property scaling empirical spatial fluctuations S(k) ~ 1/k fundamentally eliminates such EGS conceptual configurations.

The burden of the present Meq XYZM data is to get past the crustal flow modeling misapprehension that permits such extrapolations. Present UtahForge Meq XYZM data are direct evidence of fundamental spatial flow complexity at all scales that straightforwardly invalidates present UtahForge flow modeling assumptions that crustal flow structures are at most incidentally correlated. Computational models such as Fig 13 should be logically unthinkable when expressed in terms of crustal flow properties that derive from UtahForge Meq XYZM spatial correlation data.

The key perception of UtahForge XYZM spatial correlation systematics is that Meqs are intimately connected to the crustal permeability structures given by the empiric $\kappa(x,y,z) \sim \exp(\alpha\varphi(x,y,z))$. Through the Meq ~ Permeability duality, Meqs are a tool -- perhaps the only tool -- by which UtahForge can scientifically observe, understand, monitor, and potentially control the development of an EGS geothermal heat exchange volume.

USING AMBIENT CRUST MEQ ~ PERMEABILITY DUALITY IN THE UTAHFORGE HEAT EXCHANGE VOLUME

The EGS dynamic of spatially uncorrelated crust comprises (i) planar fracture dislocation surface creation by propagating stress singularities in a continuum approximation to crustal elastic moduli, combined with (ii) fluid flow according to "cubic law" volumetric rate $hV(x) \propto h^3$ that scales with the cube of the fracture aperture h. The cubic law follows directly from Poiseuille's law of planar flow $V(x) = h^2/12\mu\ \partial_x P(x)$ [9].

Unlike the above tight quantitative size and spatial correlation distributions relating UtahForge Meqs to crustal permeability obtained from well-log, well-core and well-flow empirics, present stimulation flow modeling is based the vague untested supposition that supposed UtahForge stimulation fracture creation has generated the observed Meqs. Moreover, stimulation flow modeling such as it is defaults to uncorrelated random fracture/fault parameterisation. Ipso facto, modeling confined to default spatial uncorrelations cannot reproduce the XYZM spatial correlation systematics, much less systematically relate observed spatial correlations to rock-fluid interaction spatial correlations observed in the ambient crust.

The observed Meqs size/location distribution congruence with ambient crust permeability size/location distributions allows a degree of fluid injection simulation via high-pressure fluid reactivation of pre-existing poro-connectivity pathways attested by ambient crust well-log, well-core and well-flow empirics worldwide. Fig 14 Stage2 and Stage 3 Meq XYZM data plots show the location of background Meqs (blue dots), the largest moment events (red dots) in relation to the injector source (green disk); Fig 15 displays the spatial-correlation-specific lognormal moment distributions that define the Fig 14 moment scale criteria for the red-dot/blue-dot event location distributions.

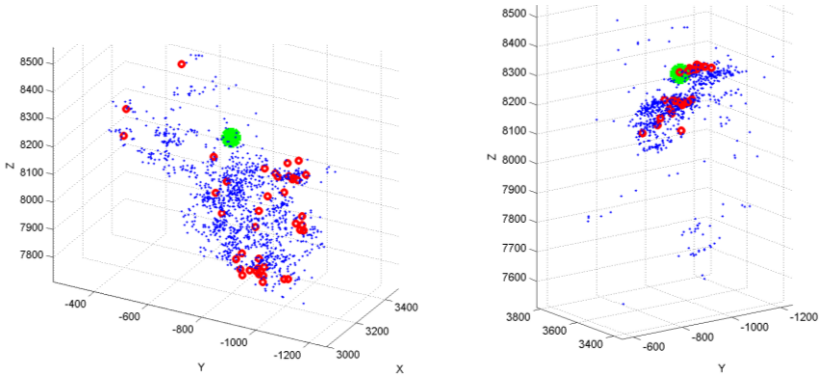

Figure 14: Spatial distribution of UtahForge Stage 2 (left) and Stage 3 (right) stimulation Meq events in relation to initial Meq given as green circle. As per Fig 15, red circles denote the largest events with blue dots denoting all remaining events. The event distributions are highly heterogeneous. Large numbers of small events occur without evident relation to large evens, while large events cluster without particular reference to small events. Stage 2 events, generated by low viscosity fluid, occur with little reference to the injection point given in green, as if injected fluid pass into the crustal volume in all directions without triggering slip events until the fluid reaches a pre-existing zone of instability. Stage 3 events, generated by viscosity 25 times greater than Stage 2 events, are more structured, as might be expected if a more viscous fluid naturally favours a subset of more porous rock with greater permeability. It is possible that the concentrated Stage 3 dislocations trigger the remote small Meqs that may well not be reached by injected fluids.

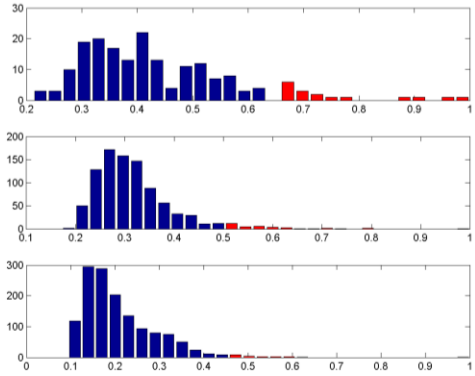

Fig 15 -- Normalised lognormal distributions of UtahForge Stage 1 (top), Stage 2 (mid) and Stage 3 (bottom) stimulation Meq event moments M ~ exp(m) given by XYZM event magnitudes m. Red bars for Stage 2-3 distributions indicate the red event locations given in the above figure spatial and below figure temporal event location displays.

The Fig 14 Meq spatial irregularities translate into the irregular time-progressions of stimulation Meqs shown in Figs 16-17. Again, in Fig 16 small red dots denote larger Meq events amidst the blue dot background emissions, with large red dots denoting the largest Meqs for each stimulation. Events are located by event occurrence on the vertical axis and by the elapsed time for each event on the horizontal axis. It is clear that the large events do not occur regularly in time.

It may be supposed that propagating fracture fronts encounter in a sequence of quasi-uniform "effective continua" that introduce spatial irregularity. A stronger assessment of spatial irregularity is, however, worth noting. Fig 17 shows the two-point correlation statistics of the Fig 16 observed Meq emission temporal irregularity in the upper three panels. While the statistical profile of Stage 1 temporal fluctuations is erratic, Stages 2 and particularly Stage 3 profiles show a steady decline in event bunching with increasing elapsed fluid injection over time.

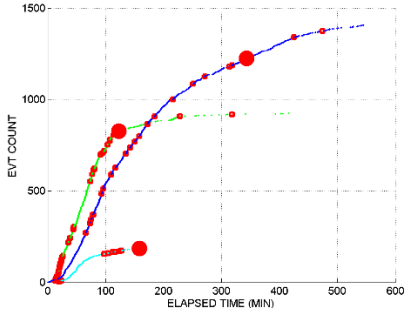

Fig 16 -- Temporal distribution of UtahForge Stage 1 (cyan), Stage 2 (green) and Stage 3 (black) stimulation Meq events in relation to initial Meqs at origin. The horizontal axis marks event times elapsed from the initial event; the vertical axis marks the event count in elapsed time. Red disks mark the largest magnitude event of each sequence; red circles mark the larger events as per Fig 15 lognormal moment distributions. The erratic temporal distributions of the largest events are evidence of significant spatial inhomogeneity of crustal permeability.

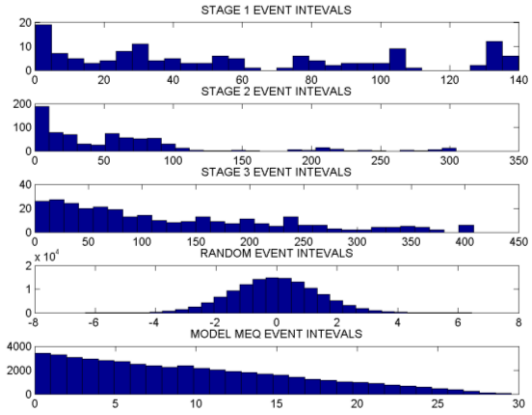

Fig 17 -- Two-point correlation function G(τ) for time lags τ between UtahForge Meq event-pairs for Stages 1-3 (top three panels), and for model radial fluid flow through 3D white and pink noise permeability structures (fourth and fifth panels respectively). While the white noise temporal correction emphatically fails to replicate the observed temporal correlation distribution, the pink noise temporal correlation replicates the steady decline with temporal offset seen in the Meq temporal sequences. The limited duration and spatial irregularity of Stage 1 flow needs considerable model adaptation to reproduce observation, but the longer Stage 2 and even longer Stage 3 temporal sequences more closely agree with the simple flow model; for Stage 3, the more viscous fluid homogenises actual flow to more nearly replicate the notional 3D radial flow of the model stimulation fluid. Closer agreement between observational and modeling irregularities would follow if the model event time sequence were computed for fluid flow simulation in a pink noise crustal permeability volume.

The observed decline is numerically reproduced in the lowest panel when it is assumed that the injected fluids flow uniformly outward from the injection well in the present of ambient crust poro-permeability distribution $\kappa(x,y,z) \sim \exp(\alpha\varphi(x,y,z))$. While the further away the fluid front is from the injection point, the fewer are the inter-event temporal correlations, the decline of lowest panel of Fig 17 replicates the observed Stage 2-3 declines of the 2nd and 3rd panels. By contrast, the standard default spatial non-correlation hypothesis produces the normal distribution seen in the 4th panel, thus comprehensively rejecting the default non-correlation hypothesis.

That the temporal irregularity of the observed Meqs is erratic compared with model temporal irregularity is due assuming that injected fluid moves outward uniformly; channelled flow in spatially erratic crustal permeability distributions would introduce more erratic model statistical profiles.

It appears from the above spatial and temporal stimulation systematics that UtahForge controlled fluid injection stimulations can be tracked in time and space by following Meq production as the high-pressure fluid exits the wellbore and enters the surrounding crustal volume to open pre-existing sealed/relic/fossil poro-connectivity pathways.

Of considerable general interest is the possibility, even likelihood, that reactivating presently sealed pre-existing poro-connectivity pathway is energetically favoured over doing work against confining pressures required for opening new fracture apertures as inherently supposed by present modeling.

To take this prospect a step further, Figs 18-20 show Stage 1-3 stimulation Meq spatial distributions at four equal time intervals of the stimulation observation sequence. As above, the green dot shows the initial Meq, with the smaller and larger Meqs shown as blue dots and red circles respectively.

Time evolution for Stages 1-2 with low viscosity fluid (either pure water at 0.2cP at T = 120°C or as reported treated water at 2cp) are spatially erratic as if the injected fluid moves through spatially erratic crustal permeability structures. By comparison the high viscosity fluid (reported as 50cP) of Stage 3 appears to migrate more cohesively through the permeability structure as if fluid is confined to the most permeable larger scale flow connectivity channels. As the relatively coherent Stage 3 Meq volume remains essentially the same throughout the stimulation, there is no evidence fluid progressing through a quasi-uniform medium tracking a leading-edge stress-singularity.

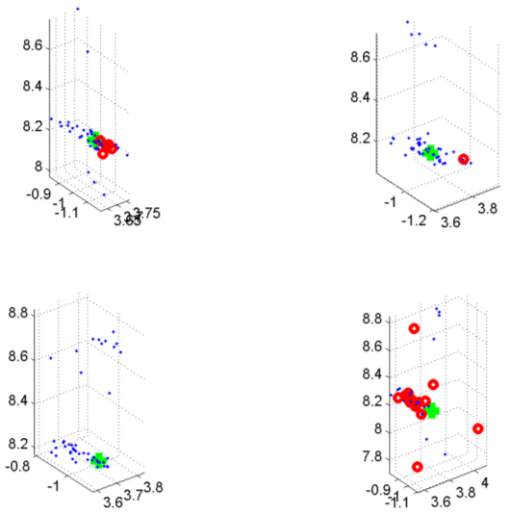

Fig 18 -- Stage 1 stimulation Meq event spatial distribution for four equal steps during the stimulation sequence. The green disk denotes position of overall the initial Meq. While during the first stimulation interval Meqs are local to the injection well, at subsequence stimulation intervals, the Meqs occur sporadically as if the stimulation fluid was following spatially erratic permeability pathways. It is notable that the majority of larger events occurs in the final stimulation interval, with half the events detached from the injection point.

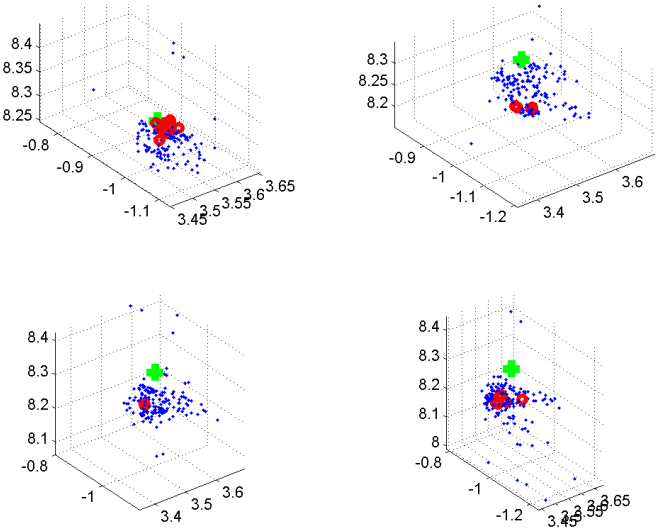

Fig 19 -- Stage 2 stimulation Meq event spatial distribution for four equal steps during stimulation. As with Stage 1, events in the first stimulation interval are local to the injection well (green disk), while for subsequent stimulation intervals events are erratically spaced as if the stimulation fluid follows permeability pathways.

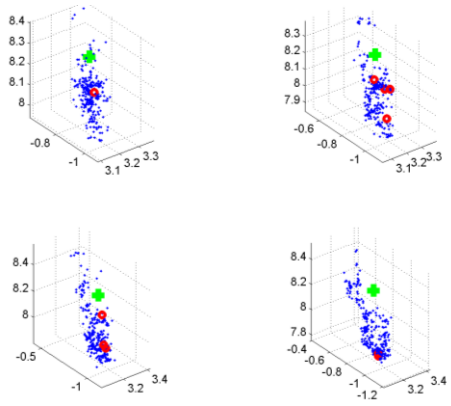

Fig 20 -- Stage 3 stimulation Meq event spatial distribution for four equal intervals during stimulation. In contrast with Stages 1-2, events in all stimulation intervals are similarly distributed in relation to the injection well (green disk). It is logical to suppose that the more viscous Stage 3 fluid is more or less confined to the most permeable of pre-existing poro-connectivity pathways accessible to the injected fluid and slowly percolates away from the main connectivity pathway. The more viscous the injected fluid the more likely that fluid is restricted to high-porosity connectivity zones in the ambient crust poroperm distribution $\kappa(x,y,z) \sim \exp(\alpha\varphi(x,y,z))$. It is unclear whether the effect of high fluid viscosity is to stimulate porosity or permeability rather than simply tracking pre-existing high poro-connectivity pathways.

SUMMARY -- UTAHFORGE MEQ SPATIAL CORRELATION CONSTRAINTS ON EGS STIMULATION PROCESS

The UtahForge Stage 1-3 stimulation Meqs are spatially correlated in two non-trivial ways:

- Meq moment distributions are lognormal;
- Meq event-pair spatial distributions are correlated with inter-pair offset, $G(r) \sim 1/r$.

Neither Meq spatial correlation empiric is consistent with the standard assumption made about spatially uncorrelation crustal reservoir fracture/fault distributions or their relation to crustal reservoir flow processes. Both Meq spatial correlation empirics, however, closely match the numerical spatial correlation properties of the crustal poro-permeability empiric $\kappa(x,y,z) \sim \exp(\alpha\varphi(x,y,z))$ arising from widely attested well-log, well-core, and well-flow data intimately associated with crustal fluids.

On present Meq XYZM evidence, it is therefore logical to

- View ambient crustal Meqs as spatially congruent with crustal permeability structures represented by $\kappa(x,y,z) \sim \exp(\alpha\varphi(x,y,z))$ for pink-noise spatially correlation porosity distribution $\varphi(x,y,z)$);
- Abandon flow stimulation models that cannot account for the observed spatial correlation properties that unite Meq data with crustal poro-permeability data;
- Strengthen surface or near-surface observational means to acquire/process Meq data that refine our understanding of EGS fluid stimulation through properly structured flow stimulation models that can support effective scientific prediction/testing of flow stimulation models.
- Follow the Meq ~ Permeability nexus and Finland EGS stimulation evidence for high frequency hHz seismic emissions to strongly aim for deploying high temperature sensors in proximity to the stimulation zone. While cylindrical sensor arrays are limited in their ability to locate events, surface sensors can perform the location function, leaving deep sensors to use temporal data to identify events for detailed broadband spectral and spatial correlation investigation of crustal flow structure $\kappa(x,y,z) \sim \exp(\alpha\varphi(x,y,z))$.